

# Two-Mode Phase Field Crystal Study of Evolution of Grain Boundaries and Dislocations in Hexagonal to Square Phase Transformation

Wu Lu<sup>1,2</sup>, Pan Rongjian<sup>1</sup>, Zhang Wei<sup>1</sup>, Chen Zheng<sup>3</sup>, Wang Heran<sup>3</sup>, Zhang Jing<sup>3</sup>

<sup>1</sup> The First Sub-institute, Nuclear Power Institute of China, Chengdu 610005, China; <sup>2</sup> National Key Laboratory for Nuclear Fuel and Material, Nuclear Power Institute of China, Chengdu 610041, China; <sup>3</sup> School of Materials Science and Engineering, Northwestern Polytechnical University, Xi'an 710072, China

**Abstract:** A two-mode phase field crystal (PFC) method was employed to focus on hexagonal to square phase transformation. Hexagonal phase with a misorientation of 6° and a tilt angle of 0°, 15°, 30°, and 45° were investigated. Results show that the hexagonal grains grow up, coalesce and form coherent grain boundaries with dislocation sets in two orientations. Square phases nucleate on these dislocation sets and their orientations are determined by dislocation sets. These square grains have two variants at each tilt angle, and the misorientations are 30°, 30°, 10°, and 5° when tilt angles are 0°, 15°, 30°, and 45°, respectively. Square grains with different orientations grow and ripen in different paces, and the grains located in preferential orientation will dominate. Dislocation sets are generated to relieve strain concentration that rises from grain growth in coherent boundaries.

**Key words:** grain boundaries; dislocation sets; square variants; phase transformation; phase field crystal

The diffusive phase transformation process consists of grain nucleation, growth and ripening as well as dislocation formation and annihilation. Such a process is decisive to mechanical and electronic properties. Phase field crystal (PFC) model is good at simulating such a process as it can catch the transient state and handle with dislocation networks on atomistic scale. The fcc, bcc, and hcp structures have the same hexagonal stacking on their close packing planes (111), (110) and (0001), and we name the hexagonal stacking in two-dimension as hexagonal phases. The (001) and (110) planes for fcc, (001) plane for bcc and hcp cylindrical plane have similar square stacking, and we name the square stacking as square phases. From this perspective, the PFC simulation of hexagonal to square phase transformation is meaningful as many materials actually exhibit this transformation, such as bcc→fcc→bcc transformation of iron, bcc→hcp transformation of titanium, and hcp→fcc transformation of zirconium.

PFC model works on atomistic scales and diffusive time

scales. It is superior in describing dislocation dynamic, grain boundary dynamic, and stress induced microstructure evolution<sup>[1-6]</sup>. Based on the PFC framework, modified versions are developed for phase transformation. PFC model is used to simulate stripe phase and triangular phase, but its single mode approximation restricts the complexity of structural transformation<sup>[7-9]</sup>. Wu et al<sup>[10-12]</sup> investigated the possibility to control the crystal symmetry within PFC and developed two-mode PFC models and they found a state of square symmetry as well as the coexistence between square phases and liquid, square phases and hexagon phases. Greenwood et al<sup>[13]</sup> used a systematic construction of two-particle correlation function that allows a broad class of structural transformation to study pure metal transformation. They further provided a detailed prescription for controlling crystal structure and introduced parameters for changing temperature and surface energy, so that phase transformation between bcc, fcc, hcp, and simple cubic (SC) lattices can be studied. It has been applied to

Received date: December 14, 2019

Foundation item: National Natural Science Foundation of China (51601185, 51704243, 51674205); Defense Industrial Technology Development Program (JCKY2017201C016); China Postdoctoral Science Foundation (2015M582575); National Key Research and Development Program of China (2016YFB07001)  
Corresponding author: Zhang Jing, Ph. D., Associate Professor, Northwestern Polytechnical University, Xi'an 710072, P. R. China, E-mail: Jingzhang@nwpu.edu.cn

Copyright © 2020, Northwest Institute for Nonferrous Metal Research. Published by Science Press. All rights reserved.

structural transformation for binary alloy<sup>[14,15]</sup>. Ofori-Opoku et al<sup>[16]</sup> extended two-point correlation kernel to ternary alloy to illustrate complex microstructure evolution in dendritic and eutectic solidification and solid-state precipitation. The above works done concerning structural transformation are inspirational for our study.

Grain growth and dislocation dynamic of phase transformation are issues yet to be clarified. Wu et al<sup>[10-12]</sup> studied grain growth using PFC, and they revealed growth mechanisms of grains with different misorientations, i.e., grain area reduction, grain rotation, and repeated faceting-defecating transition. Fallah et al<sup>[17,18]</sup> paid their attention on early stage clustering of dilute binary alloy, and found that subcritical cluster is triggered by the stress relaxation effect of quenched-in defects, such as dislocations, and subcritical clusters become overcritical due to reduction of high strain areas in the lattice. Their theoretical prediction is verified on Al-Cu real alloy with Mg addition.

Previous works provide us a good knowledge about PFC modeling on periodical lattice structure and defects. In this study, two-mode PFC was applied to study defects, morphology, and boundary migration involved in phase transformation. The PFC calculation was performed on a 512×512 matrix to obtain the density waves of each step. Graphical representation of density waves witnesses diffusive process from hexagonal phases to square phases, including grain nucleation, growth, ripening, and coalesce, also dislocations and atomic arrangement of grain boundary.

## 1 Equation of Motion

### 1.1 Free energy

Free energy of materials for PFC method is represented by a function of density waves, like crystal density field<sup>[1,19]</sup>, which can quantitatively reproduce the accuracy of real materials. The simplest PFC model has the same free-energy function as the Swift-Hohenberg model of pattern formation<sup>[7,20,21]</sup>, that is, the “one-mode” PFC model, the dimensionless form of which is given by<sup>[7,21]</sup>

$$F = \int f d\vec{x} = \int f d\vec{x} \left\{ \frac{\psi}{2} [-r + (\nabla^2 + 1)^2] \psi + \frac{\psi^2}{4} \right\} \quad (1)$$

where  $f$  is the density of free energy,  $\psi$  represents crystal density field,  $\nabla$  is the Laplace operation.

For a “two-mode” PFC model, the Helmholtz free energy is given by<sup>[7,21]</sup>

$$F^* = \int dr \left\{ \frac{\psi}{2} \left[ \alpha + \lambda(q_0^2 + \nabla^2)^2 \left[ (q_1^2 + \nabla^2)^2 + R_1 \right] \right] \psi + \frac{g}{4} \psi^4 \right\} \quad (2)$$

The dimensionless form is given by

$$F = \int f d\vec{x} = \int d\vec{x} \left[ \frac{\phi}{2} \{ -r + (\nabla^2 + 1)^2 [R_1 + (\nabla^2 + Q_1^2)^2] \} \phi + \frac{\phi^4}{4} \right] \quad (3)$$

$$R_1 = \frac{r_1}{q_0^8}, \quad r = -\frac{\alpha}{\lambda q_0^8}, \quad \psi = \phi \sqrt{\frac{g}{\lambda q_0^8}}, \quad F = \phi \frac{g}{\lambda^2 q_0^{13} F^*} \quad (4)$$

where  $r$  is dimensionless degree of undercooling;  $Q_1 = q_1/q_0$  is the ratio of two wave vector magnitudes  $q_0$  and  $q_1$  that are used to describe two sets of density waves;  $R_1$  is a parameter that controls the model stability. Contrasting Eq.(1) and Eq.(3), increasing  $R_1$  reduces the contribution of the second mode, and it reduces to the one-mode model when  $R_1 \gg 1$ . Inversely, take the extreme case as  $R_1 = 0$ , one gets the two-mode model. We used the two-mode free energy in this research.

### 1.2 Phase diagram and parameters selection

We constructed a phase diagram for liquid, square phase and hexagonal phase using classical common tangent law of free energy density.

The density of liquid  $\phi_l$  is a constant, which is written as:

$$\phi_l = \phi_0 \quad (5)$$

where  $\phi_0$  is the average atom density.

A periodical density  $\phi$  to line with crystal period was employed for solid. For square phase  $\phi_s$ :

$$\phi_s = \phi_0 + 2A_s(\cos q_s x + \cos q_s y) + 4B_s \cos q_s x \cos q_s y \quad (6)$$

For hexagonal phase  $\phi_h$ :

$$\phi_h = \phi_0 + 2A_h \left[ \cos(q_h x) \cos \frac{q_h y}{\sqrt{3}} + \cos \left( 2 \frac{q_h y}{\sqrt{3}} \right) \right] \quad (7)$$

Introduce Eq.(5~7) to free energy density of “ $f$ ” in Eq.(3), one obtains the free energy density, i.e.,  $f_l$ ,  $f_s$ , and  $f_h$  for liquid, square and hexagonal phases, respectively.

Solve equation set of partial derivatives about  $A_s$ ,  $B_s$ ,  $q_s$ , and  $q_h$  to get the expressions, and take these expressions to Eq.(7~9), one gets the minimum free energy of liquid, square phase and hexagonal phase,  $f_l(\phi_0)$ ,  $f_s(\phi_0)$ , and  $f_h(\phi_0)$ , respectively.

The common tangent construction was used to calculate the three phase diagram. In coexistence region, the chemical potentials ( $f'_i = f'_j = \mu$ ) and grand potentials ( $f_i - \mu \phi_i = f_j - \mu \phi_j$ ) of two phases are equal<sup>[8]</sup>:

$$\left. \frac{\partial f_i(\bar{\phi}_i)}{\partial \bar{\phi}_i} \right|_{\bar{\phi}_i} = \left. \frac{\partial f_j(\bar{\phi}_j)}{\partial \bar{\phi}_j} \right|_{\bar{\phi}_j} \quad (8)$$

$$\partial f_j(\bar{\phi}_j, r) - \partial f_i(\bar{\phi}_i, r) = \left. \frac{\partial f_i(\bar{\phi}_i)}{\partial \bar{\phi}_i} \right|_{\bar{\phi}_i} (\bar{\phi}_j - \bar{\phi}_i) \quad (9)$$

where  $i, j$  represents two coexistence phases.

By taking different  $r$  values between 0 and 0.6, one obtains density field  $\rho_0$  on phase boundary of liquid, square and hexagonal phase, as demonstrated in Fig.1<sup>[22]</sup>, and the parameters are chosen accordingly.

### 1.3 Diffusion equation and numerical solution

Equation of motion of PFC model has the standard Cahn-Hilliard form for conserved dynamics:

$$\frac{\partial \psi}{\partial t} = \nabla^2 \frac{\partial F}{\partial \psi} \quad (10)$$

where  $\psi$  represents crystal density field,  $t$  is the time variable,  $\nabla$  is the Laplace operation and  $\nabla^2$  operator ensures that the crystal density field is conserved.

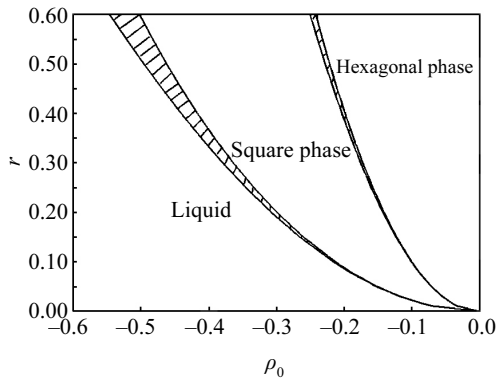


Fig.1 Two-dimensional phase diagram calculated in a two-mode PFC model (shadow represents the two-phase coexistence region)

**1.4 Applied stress and deformation**

The “deformation” abides isovolumetric hypothesis, in which the area fulfills the following conditions:

$$S = \Delta x \Delta y = \Delta x' \Delta y' \tag{11}$$

where  $\Delta x$  and  $\Delta y$  are the starting space steps,  $\Delta x'$  and  $\Delta y'$  are space steps after deformation (as shown in Fig.2).

The space step variable  $d$  fulfills  $d = \dot{\epsilon} \Delta x \Delta t$  along  $x$  direction, where  $\dot{\epsilon}$  is a dimensionless strain rate,  $\dot{\epsilon} = 6.5 \times 10^{-6} / \Delta t$  in this study. The space step is written as follows, and  $n$  is the time step:

$$x' = \Delta x + n \dot{\epsilon} \Delta x \Delta t \tag{12}$$

$$y' = \frac{\Delta x \Delta y}{\Delta x'} = \frac{\Delta y}{1 + n \dot{\epsilon} \Delta t} \tag{13}$$

**2 Results and Discussion**

The PFC calculation is performed on a  $512\Delta x \times 512\Delta y$  matrix with periodical boundary condition applied to Cartesian coordination. Three hexagonal seeds are pre-placed

on the matrix, which locate at  $0 < y < L_y/4$ ,  $L_y/4 < y < 3L_y/4$ , and  $3L_y/4 < y < L_y$ . Each of them tilts  $3^\circ$ , so the misorientation of two adjacent seeds is  $6^\circ$ . The time step is  $t=0.5$  while space step is  $\Delta x = \Delta y = \pi/4$ . The whole process comprises two steps, i.e., a preliminary solidification at higher temperature and a subsequent phase transformation at lower temperature. The first step is a relaxation process as the hexagonal phases grow up by depleting liquid phase. The second step is a deformation and phase transformation process as stress is applied. Applied stress and reduced temperature will trigger hexagonal to square phase transformation. Totally four such species having  $0^\circ, 15^\circ, 30^\circ$ , and  $45^\circ$  tilt angles (denoted as  $\delta$ ) are checked. Fig.3 presents the GB- $\theta$ - $\delta$  (grain boundary, GB) relation and the morphologies for the first step and second step.

When the hexagonal phases are stable for the first step, applied stress is introduced and the temperature decreases to the square phase region for the second step. Square phases nucleate on dislocations at the beginning and grow up by depleting hexagonal phase. Square grains SI and SII (Fig.4c) are distinguished by their orientation, and they align alternatively along hexagonal grain boundary. The included angle between [01] axis of SI and  $x$  axis is  $105^\circ$  and that for SII is  $75^\circ$ . SI grains grow rapidly along their [01] and [10] directions. SII grains align between SI gaps. They both grow separately. Growth of SII grains is somewhat suppressed by SI grains when they meet at the top boundary. At the bottom

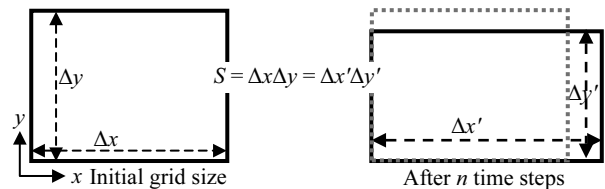


Fig.2 Schematic representation of isovolumetric deformation

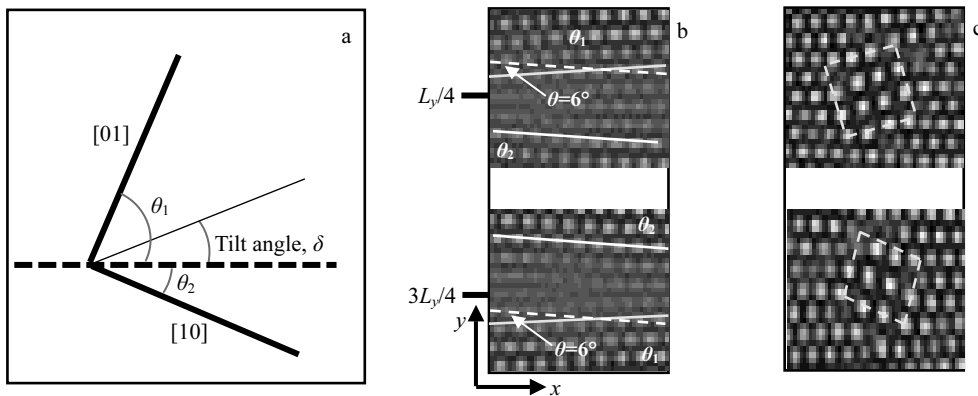


Fig.3 Schematic representation of GB- $\theta$ - $\delta$  relation (a), misorientation for a symmetrical boundary during higher temperature relaxation with  $\theta=6^\circ$  and  $\delta=0^\circ$  (b), and phase transition during low temperature deformation (square phases nucleate on dislocation) (c)

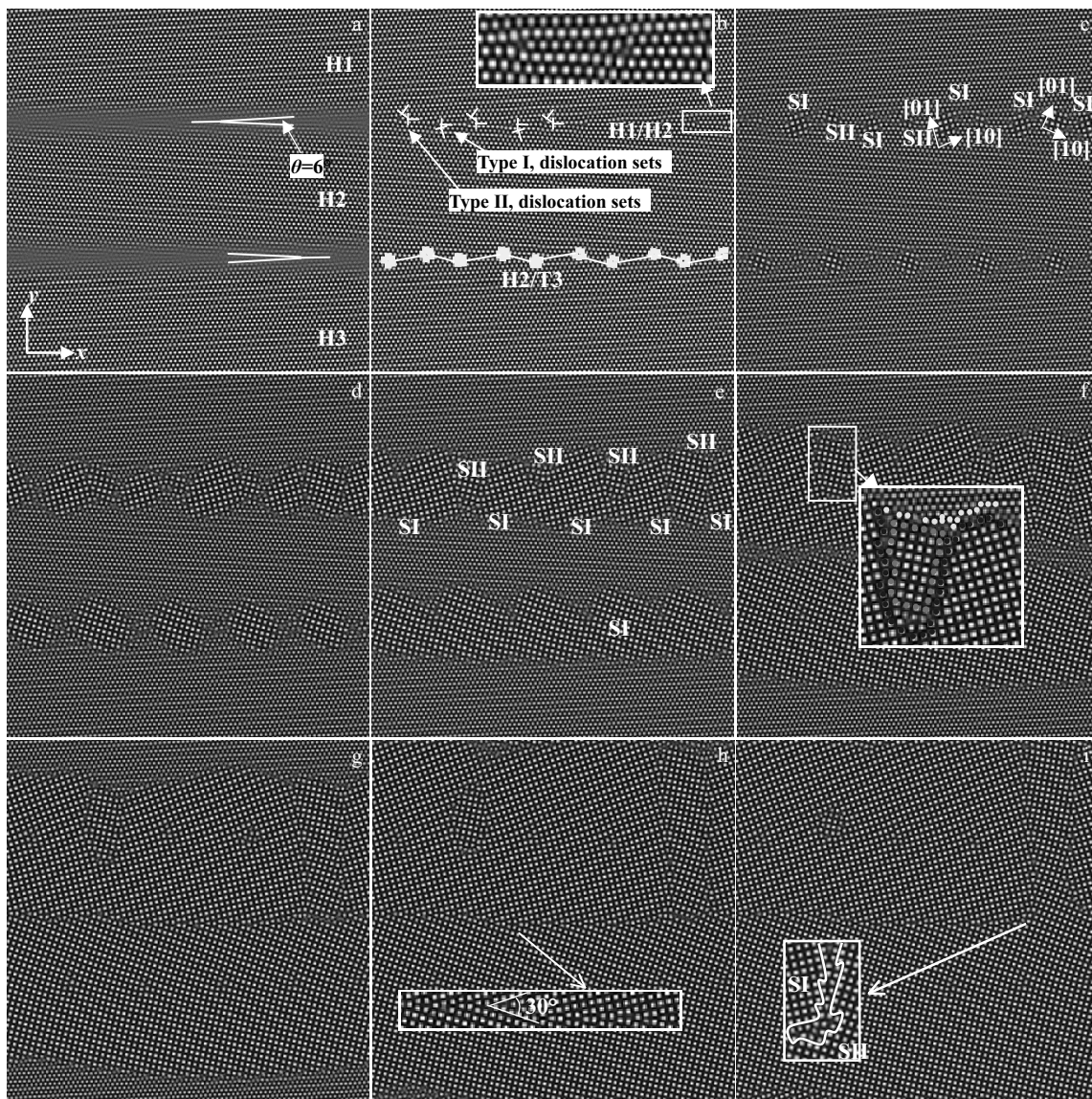


Fig.4 Hexagonal phase to square phase transformation for symmetrical grain boundary with  $\theta=6^\circ$  and  $\delta=0^\circ$ : (a) 30 and (b) 30 000 time steps for hexagonal growth; (c) 750, (d) 1020, (e) 1170, (f) 1440, (g) 1650, (h) 1980, and (i) 2430 time steps for square grains growth

boundary, growth of SI grains is suppressed by SII grains. The equilibrium morphology is predominated by SI grains with a small fraction of SII grains on the top half, but SII grains dominate with a small fraction of SI grains on the bottom half, as shown in Fig.4c~4i.

Square phases nucleate on dislocation, grow up by depleting hexagonal phase, ripen by incorporating square phases with the same orientation, and coalesce square phases with different orientations. According to the classic “nucleation→growth→ripening→coalesce” processes, the phase transformation can be concluded as the following three paths: first, hexagonal phases→square phases (SI or SII); second, hexagonal phases→square phases SI→square phases SII; third, hexagonal phases→square phases SII→square phases SI. It is

noticed that the two variants of square phase, SI and SII, inhomogeneously nucleate on two different dislocation sets, grow separately, and ripen via the second path on top and the third path at bottom.

For the H1/H2 grain boundary locates on the top half, growth of SII grains along  $[0\bar{1}]$  axis is completely suppressed, and some of them coalesce with grain SI via the second path, as demonstrated in Fig.4f. With prolonging the time, H1/H2 boundary transforms into SI/SII, SI/H, SII/H boundary type. The blue, green, and yellow dots in Fig.4f represent the constituent atoms in SI, SII and H grain, respectively. Some of these atoms on SI/SII boundary are pertained by SI or SII grain exclusively, some of these atoms are pertained to the both, and such semi-consecutive feature agrees with semi-coherent grain

boundary. Because of large size difference and dissimilar crystal structures between square phases and hexagonal phases, atoms on SI/H or SII/H align disorderly and non-consecutively, so the two are entitled as incoherent boundary. For H2/H3 boundary, the phase transformation process is basically the same with that of H1/H2. Square phases nucleate on two different dislocation sets, and form two variants: one points to  $105^\circ$  direction and the other points to  $75^\circ$ . SII grains are on prevail while SI grains are suppressed. Final misorientation of SI and SII is  $30^\circ$  with semi-coherent boundary.

The tilt angle is enhanced to  $15^\circ$ , and the diffusive process of phase transformation is shown in Fig.5. Dislocation sets are generated when two adjacent hexagonal phases coalesce. Each one comprises two edge dislocations with a  $60^\circ$  included angle, and all line on hexagonal subgrain boundary regularly. Analogously, these dislocation sets have two orientations, which will determine the square phases to nucleate on them. Atoms on hexagonal subgrain boundary are ordered, consecutive, and coherently bonded, which agree with the features of coherent boundary. Square phases nucleate on dislocation sets and form two square variants, SI and SII, of which the former points to  $60^\circ$  and the later points to  $30^\circ$ . Partial enlarged details of SI/H and SII/H are given by Fig.5c. The hetero- phase boundaries of square phases and hexagonal phases are disordered, non-consecutive, and ill-bonded, thus titled as incoherent

boundary. These high-angle hetero grain boundaries are in irregular zigzag-like shape but become smooth gradually, as show in Fig.5e and 5f. Some of these atoms on SI/SII boundary are pertained to SI or SII exclusively, and some are pertained to the both, featured as semi-coherent boundary.

With further enhancement of the tilt angle to  $30^\circ$ , the morphology evolution is demonstrated in Fig.6. H1/H2 and H2/H3 grain boundaries are coherent and there are dislocation sets in  $60^\circ$  included angle. Square phases nucleate on dislocation sets, and these square phases have very small misorientation. Square phases ripen and coalesce with distorted lattice nearby the junction, so the whole grains are in a strained state. Square phases grow up along their [01] direction with slightly adjusting their orientation, and such adjustment causes the final square phases to grow in two directions, i.e., SI grain points to  $40^\circ$  direction and the SII grain points to  $50^\circ$  direction (Fig.5f). Atoms on SI/SII grain boundaries line orderly and consecutively, and dislocation sets and single dislocation are inevitably generated to relieve the coherent strain.

Calculation for  $45^\circ$  tilt angle is carried out, and the microstructures are depicted in Fig.7. The starting hexagonal grain boundaries consist of dislocation sets. Square phases nucleate on dislocation sets, and one points to  $65^\circ$  and the other points to  $90^\circ$ . SI and SII grains grow up and ripen competitively, and SI grains dominate eventually by depleting SII grains. During

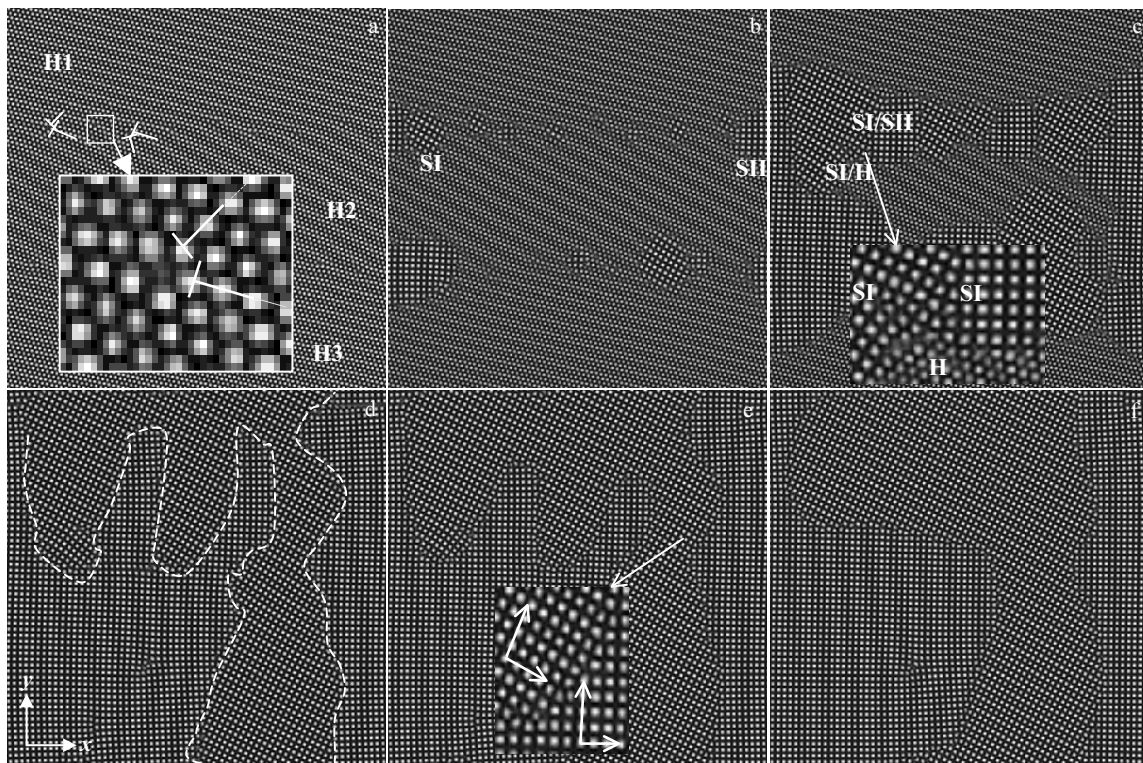


Fig.5 Hexagonal phase to square phase transformation for symmetrical grain boundary with  $\theta=6^\circ$  and  $\delta=15^\circ$ : (a) 30 000 time steps for hexagonal grain growth; (b) 990, (c) 1500, (d) 2400, (e) 3300, and (f) 30 000 time steps for square grain growth

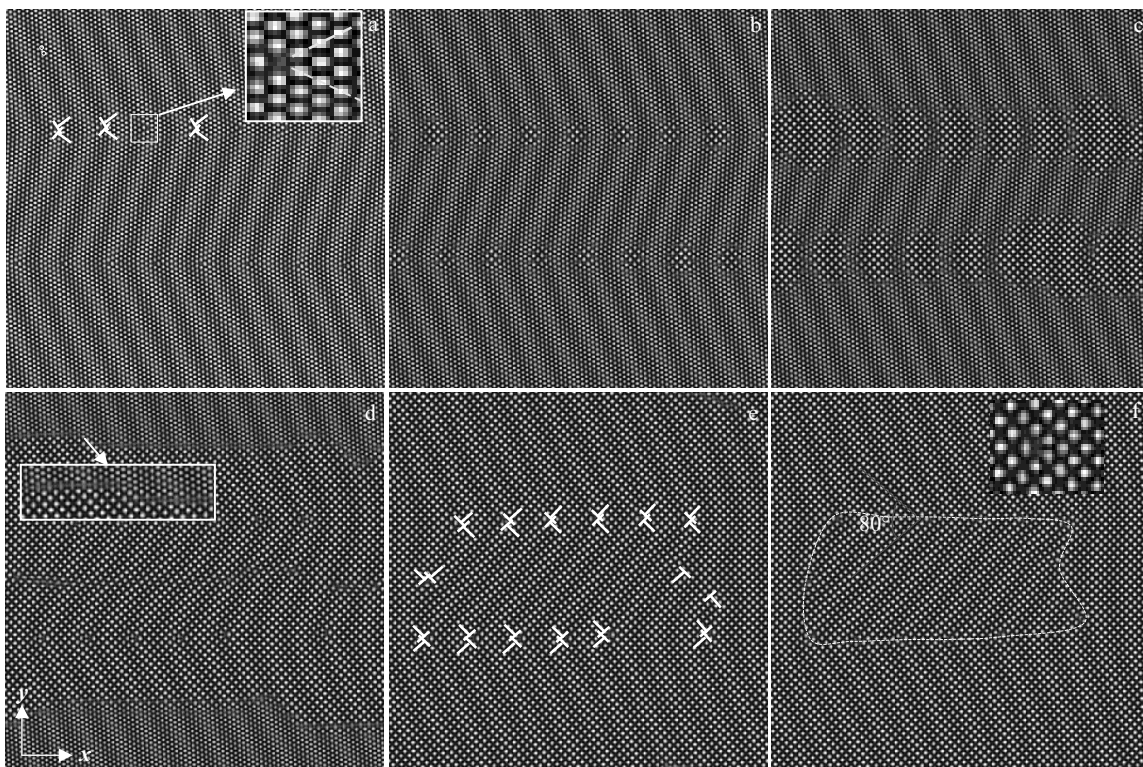


Fig.6 Hexagonal phase to square phase transformation for symmetrical grain boundary with  $\theta=6^\circ$  and  $\delta=30^\circ$ : (a) 30 000 time steps for hexagonal grain growth; (b) 750, (c) 1140, (d) 1500, (e) 2010, and (f) 4050 time steps for square grain growth

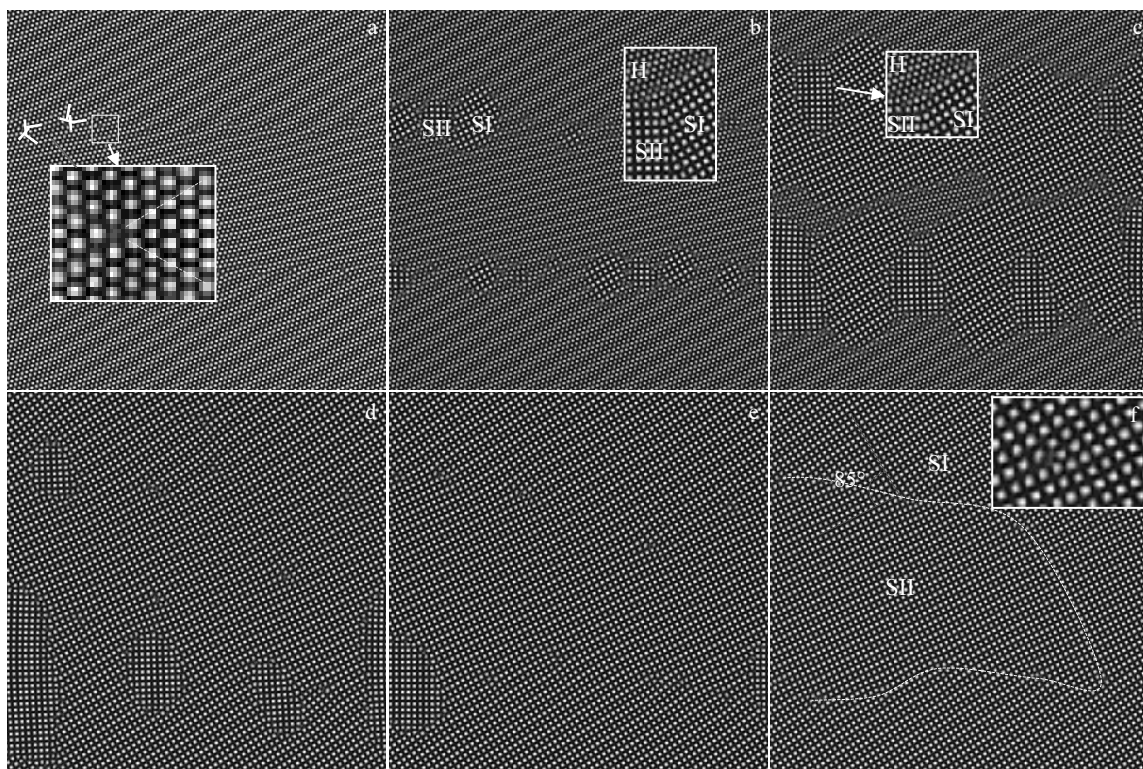


Fig.7 Hexagonal phase to square phase transformation for symmetrical grain boundary with  $\theta=6^\circ$  and  $\delta=45^\circ$ : (a) 30 000 time steps for hexagonal grain growth; (b) 900, (c) 1500, (d) 3000, (e) 10 500, and (f) 24 000 time steps for square grain growth

ripening and coalesce process, some SI grains adjust their orientation to reduce system energy; we name this kind of grain as SIII. The final microstructures consist of SI and SIII grains with a misorientation of 5°, as shown in Fig.7f. SI/SIII grain boundaries are ordered, consecutive, and belong to coherent boundary.

Fig.8 provides a comparison of bicrystal and tricrystal grain boundaries for H/H and S/H with various  $\delta$ , and the corresponding data is summarized in Table 1. Let's start with hexagonal subgrain boundary. Hexagonal phases nucleate at the beginning with a misorientation of 6°, then grow up, ripen and coalesce, and develop into coherent subgrain boundary aligned with regularly spaced dislocation sets. A perfect

hexagon structure is characterized by six-membered ring with one in the center (red dot line in Fig.8a). Dislocation sets are characterized by five-membered ring due to missed atom at the end of dislocation (green dot line in Fig.8a). For each tilt angle case connecting these rings into hexagon and pentagon, the orientation of grain and dislocation can be distinguished, which indicates obvious grain rotation with varied tilt angle. Besides that, grain rotation in a constant tilt angle is also observed as the hexagonal phase adjusts its orientation to fit each other better. Misorientation causes strain growth, and strain concentration accumulated in grain growth is relieved by dislocation or grain rotation.

Square phases and hexagonal phases differ in crystal struc-

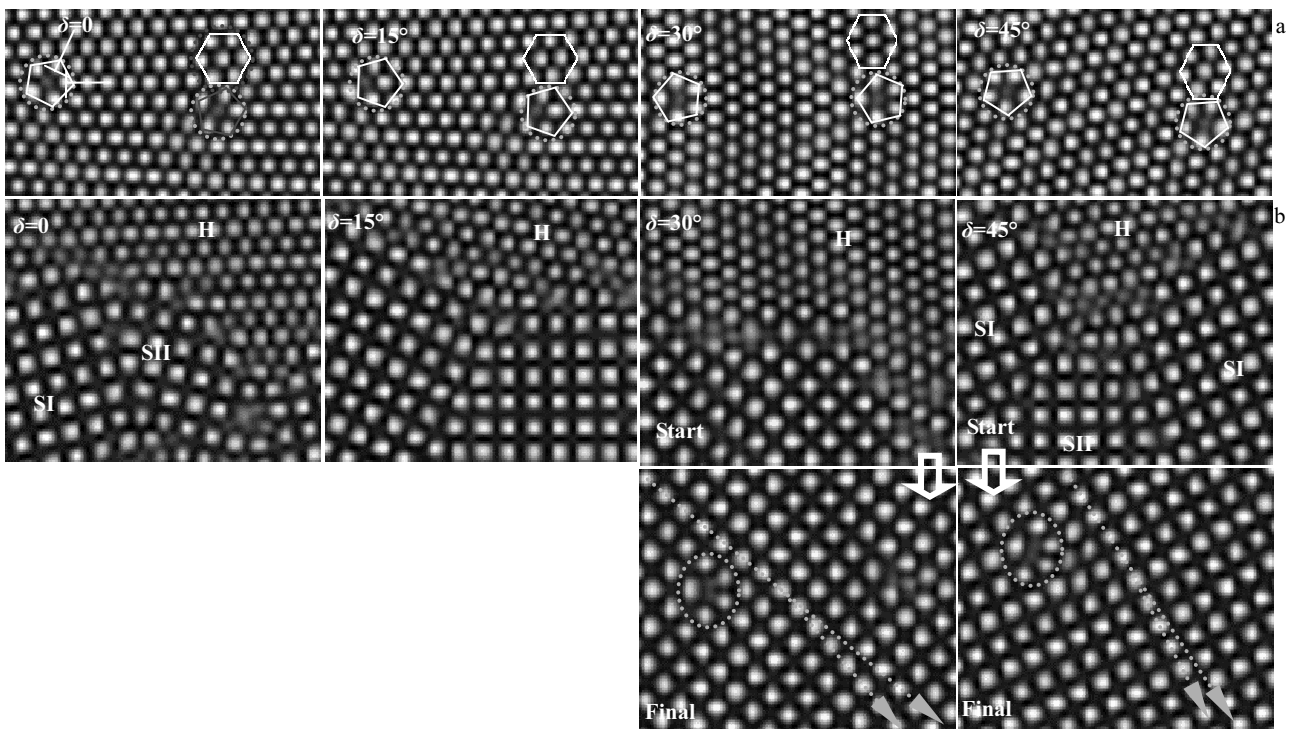


Fig.8 Hexagonal/hexagonal grain boundary (H/H) and the five-atom-cycle as a result of vacancy on dislocation end (a); square/hexagonal bi-/tri-grain boundary (S/H) and square/square (S/S) grain boundary (b)

**Table 1** Boundary type and misorientation of square phases with  $\theta=6^\circ$  and tilt angles  $\delta=0^\circ, 15^\circ, 30^\circ, 45^\circ$

$\delta/(\circ)$	H/H	SI/H&SII/H	SI/SII	SI/ $(\circ)$	SII/ $(\circ)$	Misorientation/ $(\circ)$
0	C	I	S	105	75	30
15	C	I	S	60	90	30
30	C	I	C	50	40	10
45	C	I	S*	Start: 65*	90*	25*
			C*	Final: 28*	33*	5*

Note: \* indicates that the orientation of square phases changes with time; H is hexagonal phase; SI and SII represents square grains in two different orientations; H/H, SI/H, SII/H, and SI/SII represent the grain boundaries of two grains; C: short for coherent; I: short for incoherent; S: short for semi-coherent

ture and lattice parameter, so it is easy to understand that S/H grain boundaries are incoherent. Such a boundary is characterized by random arranged atoms and large surface areas. S/H boundaries are formed when square phases nucleate on dislocation sets during hexagonal phase to square phase transformation. The incoherent S/H hetero-boundaries themselves bring little strain, but semi-coherent or coherent S/S homo-boundaries will introduce strain during ripening and coalescing. The strain concentration can be relieved by either surface or dislocation, and for the S/H boundaries, strain concentration is relieved by surface.

Square phases nucleate on dislocation sets, and their orientation is determined by dislocation sets. Two kinds of square grains generally align alternatively along hexagonal subgrain boundaries. For tilt angles of  $0^\circ$  and  $15^\circ$ , square phases nucleate with a misorientation of  $30^\circ$  from the beginning, and such high-angle semi-coherent grain boundaries assure that stress can be released thoroughly and timely by surface, so square phases grow up without rotation to adapt to each other. For tilt angle of  $30^\circ$ , the square phases grown in a certain misorientation can make sure a perfect coherent bonding of the two square variants but lead to severe stress concentration during coalescing. Therefore, square phases rotate to adapt to each other, resulting in a final misorientation of  $10^\circ$ . For tilt angle of  $45^\circ$ , though there is a large misorientation from the beginning, one grain dominates, ripens and coalesces the other thoroughly. This process causes very small strain concentration on grain edge, leading to a small misorientation ( $5^\circ$ ) for the final square phases. Certainly, strain is also relieved by generating sparse dislocation lastly.

### 3 Conclusions

1) If tilt angle  $\delta$  equals  $0^\circ$ , hexagonal grains grow from liquid in a symmetrical way. These grain boundaries bond consecutively, with two types of dislocation sets aligning a constant interval. When the tilt angle  $\delta$  is enhanced to  $15^\circ$ ,  $30^\circ$ , and  $45^\circ$ , these grain boundaries are asymmetrical, but still coherently bonded and distributed with two types of dislocation sets. Hexagonal grain rotation is observed, and it is generally a way to release the strain concentration arising from lattice mismatch because of misorientation. Besides that, another effective way is generation of dislocations.

2) Square phases nucleate on dislocation sets and grow into directions determined by dislocations sets, thereby forming two variants. Competitive growth of two variants is restrained by each other, leading to unbalanced fraction in the final morphology. Square phases in two directions coexist with misorientations of  $30^\circ$ ,  $30^\circ$ ,  $10^\circ$ ,  $5^\circ$  for tilt angles  $\delta$  of  $0^\circ$ ,  $15^\circ$ ,  $30^\circ$ ,  $45^\circ$ , respectively. Dislocation sets also exist on square grain boundary when angles are  $30^\circ$  and  $45^\circ$ .

3) Hexagonal grain boundaries are coherent because of

perfect lattice matching, and dislocation sets are generated on the boundaries to release coherent strain. Hexagonal/square grain boundaries are incoherent because of large lattice mismatch. Square/square grain boundaries are coherent under low misorientation conditions and semi-coherent under high misorientation conditions.

### References

- Berry J, Elder K R, Grant M. *Physical Review B*[J], 2008, 77(22): 224 114
- Adland A, Karma A, Spatschek R et al. *Physical Review B*[J], 2013, 87(2): 24 110
- Zhao Y H, Zhang B, Hou H et al. *Journal of Materials Science & Technology*[J], 2019, 35(6): 1044
- Gránásy L, Tegze G, Tóth G I et al. *Philosophical Magazine*[J], 2011, 91(1): 123
- Provatas N, Dantzig J A, Athreya B et al. *JOM*[J], 2007, 59(7): 83
- Guo Huijun, Zhao Yuhong, Sun Yuanyang et al. *Superlattices and Microstructures*[J], 2019, 129: 163
- Elder K R, Katakowski M, Haataja M et al. *Physical Review Letters*[J], 2002, 88(24): 245 701
- Jaatinen A, Ala Nissila T. *Journal of Physics: Condensed Matter*[J], 2010, 22(20): 205 402
- Qi Kewu, Zhao Yuhong, Guo Huijun et al. *Acta Physica Sinica*[J], 2019, 68(17): 170 504
- Wu K A, Voorhees P W. *Physical Review B*[J], 2009, 80(12): 125 408
- Wu K A, Adland A, Karma A. *Physical Review E*[J], 2010, 81(6): 61 601
- Wu K A, Voorhees P W. *Acta Materialia*[J], 2012, 60(1): 407
- Greenwood M, Provatas N, Rottler J. *Physical Review Letters*[J], 2010, 105(4): 45 702
- Greenwood M, Rottler J, Provatas N. *Physical Review E*[J], 2011, 83(3): 31 601
- Greenwood M, Ofori-Opoku N, Rottler J et al. *Physical Review B*[J], 2011, 84(6): 64 104
- Ofori-Opoku N, Fallah V, Greenwood M et al. *Physical Review B*[J], 2013, 87(13): 134 105
- Fallah V, Stolle J, Ofori-Opoku N et al. *Physical Review B*[J], 2012, 86(13): 134 112
- Fallah V, Ofori-Opoku N, Stolle J et al. *Acta Materialia*[J], 2013, 61(10): 3653
- Shen Y C, Oxtoby D W. *The Journal of Chemical Physics*[J], 1996, 105(15): 6517
- Elder K R, Grant M. *Physical Review E*[J], 2004, 70(5): 51 605
- Swift J, Hohenberg P C. *Physical Review A*[J], 1977, 15(1): 319
- Yun Jiangjuan, Chen Zheng, Li Shangjie. *Acta Phys Sin*[J], 2014, 63(9): 98 106 (in Chinese)

## 双模晶体相场研究六方四方相变过程中晶界和位错演化

吴璐<sup>1,2</sup>, 潘荣剑<sup>1</sup>, 张伟<sup>1</sup>, 陈铮<sup>3</sup>, 王贺然<sup>3</sup>, 张静<sup>3</sup>

(1. 中国核动力研究设计院 第一研究所, 四川 成都 610005)

(2. 中国核动力研究设计院 核燃料及材料国家重点实验室, 四川 成都 610041)

(3. 西北工业大学 材料学院, 陕西 西安 710072)

**摘要:** 采用双模晶体相场法研究六方相向正方相的转变。分别针对倾侧角为 0°、15°、30°和 45°，晶粒取向差为 6°的六方相体系做了研究。结果表明：六方晶粒长大、溶合、并形成共格晶界，位错组沿六方晶界均匀分布，并有 2 种取向。正方相在位错组处形核，并且其取向取决于位错组取向。每一种倾侧角的体系中均形成 2 个取向正方相的变体。针对倾侧角为 0°、15°、30°和 45°的六方相体系，生成的四方相变体之间的取向差分别为 30°、30°、10°和 5°。不同取向的正方相晶粒长大熟化的方式有差异，位于有利取向的晶粒将会优先生长并占据主导地位。以共格晶界形式长大的晶粒，晶界处有位错组生成以松弛晶粒长大的应力集中。

**关键词:** 晶界；位错组；正方相变体；相变；晶体相场

---

作者简介: 吴璐, 男, 1985 年生, 博士, 研究员, 中国核动力研究设计院第一研究所, 四川 成都 610005, E-mail: wulu1002@qq.com